Application of multiphase computational fluid dynamics to the plasma arc impingement problem in DC furnaces

Quinn G. Reynolds[1*]

[1]Mintek, Private Bag X3015, Randburg, 2125, South Africa

quinnr@mintek.co.za

Abstract: Direct-current (DC) plasma arc furnaces are a key unit operation in many modern metallurgical production processes. The plasma arc takes the form of a jet of hot ionised gas, which interacts strongly with the molten process material (typically consisting of light slag and dense metal liquid phases) inside the furnace vessel. A good understanding of the flow patterns and in particular the size and shape of the cavity formed in the interaction zone between arc and molten material is important for accurate calculation of power supply specifications during the design of DC furnaces. In the present study, the arc is approximated as a simple gas jet using relationships between the thrust generated by the jet and the electrical parameters of the furnace. Similarity considerations are then used to construct a computational model system consisting of a gas jet interacting with a two-phase fluid, which is simulated using volume-of-fluid based methods. Transient solvers are used to study the development of the model system from stagnant initial conditions, and the impact on furnace design and operational behaviour at different scales is considered.

Keywords: pyrometallurgy, electric furnace, multiphase, computational fluid dynamics

INTRODUCTION

The direct-current (DC) plasma arc furnace is a type of electric furnace design used for pyrometallurgical processing of materials, generally to produce a metal product. DC furnaces have been used extensively in the steel recycling industry, and more recently have found application in the reductive smelting of mined ores to produce ferrochromium, titania slag, ferronickel, and other commodities (Jones & Curr [1]).

A schematic of a typical DC furnace is shown in Figure 1. The furnace consisits of a cylindrical containment vessel lined with various refractory materials and cooling elements. Raw material (ore, chemical modifiers, and carbonaceous reductants) is fed through several openings in the vessel roof. A single graphite electrode enters through the roof of the vessel. The tip of the electrode is positioned some distance above the surface of a pool of molten process material, and a plasma arc is formed between the tip and the surface. The arc is the primary heating and stirring element in the furnace. It converts electrical power which is supplied to the furnace via transformers and DC rectifiers, into thermal energy for melting and reaction of the raw materials. The pool or “bath” of molten material consists of at least two immiscible liquid phases – usually a denser metal phase below a lighter slag (oxide material) phase.

The arc is a high-velocity, high-temperature jet consisting of plasma, material in the fourth state of matter. Plasmas are an electrically-conductive mixture of neutral atoms and molecules, positive ions, and negative electrons which form when gases are heated to high temperatures (> 7 000 K). The arc is a magneto-hydrodynamic (MHD) system, sustained by strong interactions and coupling between the velocity, temperature, and electromagnetic fields it generates (e.g., Alexis et al. [2]).

Passage of electric current through the arc inputs energy and maintains the temperatures necessary for ionization via resistance heating. This is balanced by energy loss processes, including volumetric radiation and convection to the molten bath surface below. The majority of the thermal energy in the arc is delivered into the interaction region at the surface of the slag bath, making it a very efficient means of heating the process material. Flow of plasma in the arc column is driven strongly by self-induced electromagnetic Lorentz forces – these result from the constriction of the conduction channel in the region where the arc attaches to the graphite electrode. This constriction causes the arc to draw in gas from the surroundings where it is heated and accelerated away from the electrode surface, toward the molten bath below (Maecker [3], Bowman [4]).

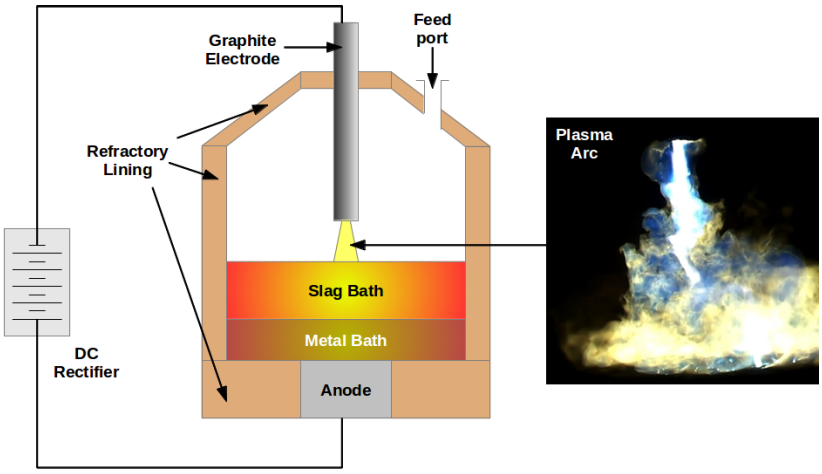

Figure 1: Diagram showing principal components of a typical DC arc furnace

Fluid-dynamic and electromagnetic instabilities are common in plasma arcs due to the large driving forces and shear gradients present, and cause turbulent flow and dynamic behaviour of the arc jet (Bowman [4], Reynolds et al. [5]). Instabilites may also result from the continual ablation and erosion of the graphite electrode by the hot plasma; these can cause the arc to "jump", or rapidly change position and direction on the electrode surface. This behaviour often results in the arc jet pointing onto a different and relatively undisturbed region of the molten bath. Time scales associated with this behaviour are of the order of hundreds to thousands of milliseconds (Bowman [4]).

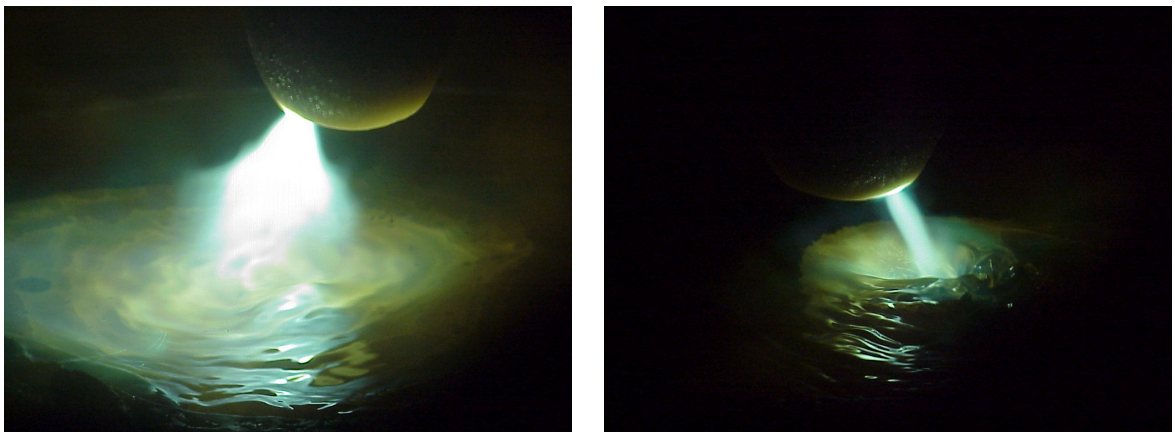

(a) (b)

Figure 2: Photographic images of (a) shallow and (b) deep cavities formed by plasma arcs on liquid slag surfaces (Jones et al. [6])

The mechanical action of the arc impinging on the surface of the molten bath can be substantial, due to the significant momentum carried by the plasma jet. This typically creates a cavity on the surface of the molten material, with vigorous flow and stirring in the immediate vicinity. Some examples are shown in Figure 2. Industry perception as to the nature of this interaction zone is highly divided; the arc may penetrate

through the slag to the underlying metal, or impart only a shallow depression on its surface. Understanding which is the case is useful for the design and operability of DC furnaces, since the arc and slag layer are connected in series to the DC power supply (see Figure 1). Both have an electrical resistance that is a function of their geometry – in the case of the slag layer, the cavity size and shape is critically important in determining this resistance (Reynolds & Jones [7]). Once the various resistances can be calculated, a specification for the furnace power supply for a particular operation can be drawn up. These power supplies are typically very expensive and difficult to modify once constructed. A means of estimating the cavity dimensions and dynamics in advance for a given furnace would therefore be of great utility in optimizing the design and enabling a better understanding of the electrical behaviour.

Study of the interaction zone formed by gas jets impinging on liquid surfaces was first approached using basic analytical and empirical models to determine the size of the cavity formed by a turbulent jet exerting a known thrust force (e.g., Cheslak [8]). Development of strong analogies between arcs and turbulent gas jets later permitted the extension of these methods to apply to DC plasma arcs (Ushio et al. [9], Bowman [4]). More recently, steady-state two-phase computational fluid dynamic studies of planar (Forrester & Evans [10]) and cylindrical (Nguyen & Evans [11]) gas jets impinging onto liquid surfaces have been performed in order to calculate the cavity dimensions and flow patterns in the interaction zone from first principles, and have yielded results in good agreement with theory and experiment.

In order to build on and extend this work, development of a computational fluid dynamics model using a turbulent gas jet of appropriate specifications to represent the arc and a liquid bath consisting of two distinct phases was deemed to be of some value for further study of the interactions between the arc and the molten bath in DC furnaces. A dynamic model, able to study the evolution of the cavity and flow patterns in time, was preferred due to the transient and erratic nature of the arc jet's position and direction of impingement.

THEORY AND MODEL DESCRIPTION

The thrust force generated by a plasma arc jet was first described analytically by Maecker [3], based on calculations of the electric and magnetic fields produced by a constriction in a plasma conductor. The Maecker expression, (1), has been experimentally confirmed for plasma arcs at currents up to 2 kA (Bowman [12]).

$$T = \frac{\mu_0 I^2}{4\pi}\left(ln\frac{r_a}{r_c} + \frac{1}{2}\right) \tag{1}$$

Here, T is the thrust force (in N), μ_0 is the permeability of free space, I is the arc current (in A), and r_a and r_c are the radii of the main body of the arc and the attachment spot on the electrode surface respectively (in m). Bowman [4] later developed an empirical shape model for the conductive body of the arc by fitting a large range of observational data. This model predicts a constant ratio between r_a and r_c across all scales of arc operation, and allows the arc thrust to be expressed as directly proportional to the square of the current.

$$T = A_T I^2, \quad A_T = 1.663\times10^{-7}\ N/A^2 \tag{2}$$

Mathematical and computational modelling of axisymmetic DC plasma arcs has indicated a substantial degree of similarity between the momentum field of the arc and that of a turbulent jet (Bowman [13]). For the purposes of this study – which is primarily focused on modelling of the interactions between the arc jet and the molten bath rather than the arc itself – the arc was therefore not described rigorously using MHD methods, but rather approximated using a simple turbulent gas jet. A key parameter is the thrust force generated, which from turbulent jet theory is given by (3).

$$T = \frac{\pi}{4}\rho u_0^2 d_0^2 \tag{3}$$

Here, ρ is the gas density, u_0 is the velocity of the gas stream at the inlet nozzle, and d_0 is the nozzle's diameter. Equivalency between (2) and (3) should be maintained in any modelling work in order for the turbulent jet to accurately describe the thrust force exerted on the surface of the molten bath by the arc.

Model region and dimensional analysis

The geometry of the axisymmetric modelled region of the furnace is shown in Figure 3a, showing the dimensions and physical properties used. The jet inlet diameter is given by d_N, the electrode diameter by d_E, and the furnace vessel diameter by d_F. The original depths of the metal and slag phases are given by h_D and h_L respectively. The length of the arc is given by L_A, and the length of the vertical section of electrode is given by L_E. ρ_i and μ_i are the density and viscosity of the separate phases, with subscripts G referring to the gas phase, L to the lighter liquid phase (slag), and D to the denser liquid phase (metal). Surface tension values at the interfaces between the phases are given by γ_{GL} and γ_{LD}. AB is the jet inlet, and BCD defines the boundaries of the electrode. DE is assumed to be open to the atmosphere inside the gas space of the furnace. EFG are solid boundaries defined by the walls of the furnace containment vessel.

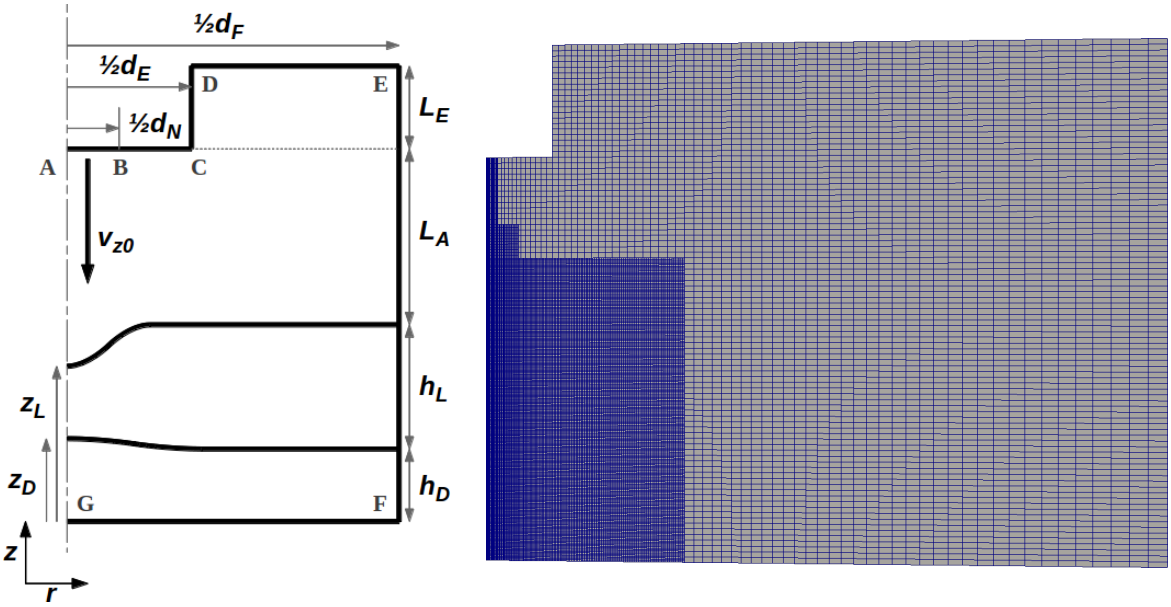

(a) (b)

Figure 3: Model region for jet impingement study, (a) diagram, (b) example mesh

DC furnaces are operated at a wide range of scales, from pilot-plant furnaces running at a few hundred amperes up to a few kA, to industrial plants using hundreds of kA. A dimensional analysis was performed using the following group of key parameters, in order to reduce the number of variables and account implicitly for scale effects in the model: L_A, h_D, h_L, d_E, d_F, ρ_G, ρ_L, ρ_D, μ_G, μ_L, μ_D, γ_{GL}, γ_{LD}, g, T. The thrust force T is used in place of the jet velocity v_{z0} and nozzle diameter d_N, as these values are not well-defined for arcs whereas the thrust may be calculated easily for either arc or gas jets using (2) and (3).

This list of parameters comprises 15 variables, using 3 fundamental dimensions. It may therefore be reduced to 12 dimensionless quantitites, shown in Table 1. This amounts to linear scaling of all dimensions between the real furnace and the model, together with ratio scaling of the physical properties of the three phases. An additional three classical dimensionless groups determine the flow behaviour of the jet representing the arc (N_{Re}), the interaction between the momentum of the jet and the momentum of the slag layer (N_{Fr}), and the relative strengths of the momentum and surface tension forces in the slag layer (N_{We}).

Dependent variables such as the position of the gas-slag and slag-metal interfaces on the centreline (denoted by z_L and z_D respectively, see Figure 3) over time, and the time of formation of any features of interest (denoted by t), must also be expressed as dimensionless quantities to account for any scaling between model and real furnace. This is done using the expressions shown in Table 2.

If the parameters of the model are chosen relative to the parameters of the real furnace such that there is numerical equivalence between all the dimensionless quantities, a strong degree of similarity in the resulting flow behaviour would be expected.

Table 1: Dimensionless parameters for multiphase flow model

Parameter	*Definition*	*Parameter*	*Definition*
Reynolds number, N_{Re}	$\sqrt{\frac{4\rho_G T}{\pi\mu_G^2}}$	Scaled metal depth	$\frac{h_D}{L_A}$
Froude number, N_{Fr}	$\frac{T}{g\rho_L L_A^3}$	Scaled slag depth	$\frac{h_L}{L_A}$
Weber number, N_{We}	$\frac{T}{\gamma_{GL} L_A}$	Scaled electrode diameter	$\frac{d_E}{L_A}$
Surface tension ratio	$\frac{\gamma_{GL}}{\gamma_{LD}}$	Scaled furnace diameter	$\frac{d_F}{L_A}$
Gas-Slag density ratio	$\frac{\rho_G}{\rho_L}$	Gas-Slag viscosity ratio	$\frac{\mu_G}{\mu_L}$
Slag-Metal density ratio	$\frac{\rho_L}{\rho_D}$	Slag-Metal viscosity ratio	$\frac{\mu_L}{\mu_D}$

Table 2: Dimensionless dependent variables for multiphase flow model

Variable	*Definition*
Dimensionless slag level	$\frac{z_L}{h_L + h_D}$
Dimensionless metal level	$\frac{z_D}{h_L + h_D}$
Dimensionless time	$\sqrt{\frac{g}{L_A}}t$

Numerical and computational approach

The multiphase jet impingement problem was implemented using the OpenFOAM [14] framework for field solution of conservation equations. The model uses OpenFOAM's existing *multiphaseInterFoam* solver, and consists of three elements: a flow model, a turbulence closure model, and a phase separation model. The equations governing the various fields are discretised for numerical solution using a finite-volume approach.

The incompressible Navier-Stokes (4) and continuity (5) equations with standard Newtonian shear stresses are used to describe the fluid flow across all phases.

$$\rho\frac{\partial \mathbf{v}}{\partial t} + (\rho\mathbf{v}\cdot\nabla)\mathbf{v} + \nabla P = \nabla\cdot\left(\mu_{eff}\nabla\mathbf{v}\right) \tag{4}$$

$$\nabla\cdot(\rho\mathbf{v}) = 0 \tag{5}$$

Here, **v** is the velocity vector field, and *P* is the pressure field. μ_{eff} is an effective turbulent viscosity, which is calculated from the fields generated by the turbulence closure model. In this case a Reynolds-averaged Navier Stokes approach using the standard two-equation *k*-ε turbulence model (Launder & Sharma [15]) is used together with wall functions to account for the gradients near to solid surfaces. Several variations of this model were tested by Nguyen & Evans [11], with the conclusion that it provides acceptable accuracy for problems of the jet impingement type.

The volume-of-fluid (VOF) method (Hirt & Nichols [16]) is used to account for the phase separation. In this method, solution of a separate convective transport equation is required for the volume fraction field of each phase, α_i – this permits the geometric shape of the phase regions and the interfaces between them to be tracked easily without the need for computationally-expensive mesh recalculations.

The Pressure Implicit with Splitting of Operators (PISO) predictor-corrector algorithm is used for calculation of the velocity and pressure fields at each time step. The k, ε, and α_i fields are solved directly as convection-only or convection-diffusion equations at each time step. Gradient-limited discretisations are used for all divergence terms with the exception of those related to the α_i fields, which use the specialised Multidimensional Universal Limiter for Explicit Solution (MULES) interface compression method. Adaptive time-stepping was used in order to maintain a Courant number of 1 or below.

Boundary conditions are supplied along the edges of the model region shown in Figure 3a. AB forms the jet inlet, with a specified constant velocity v_{z0} in the vertical direction, specified constant values of k and ε calculated from the inlet velocity and nozzle diameter, and unity gas-phase fraction. BCD forms the surface of the electrode, with zero velocity, wall function values for k and ε, and zero gradient for the phase fractions. DE is open to the atmosphere of the furnace, with velocity determined by the local pressure gradient, zero gradient for k and ε, and either unity gas-phase fraction or zero gradient for all phase fractions depending on the direction of the normal velocity. EFG forms the wall of the containment vessel, with a specified constant velocity of zero, wall function values for k and ε, and zero gradient for the phase fractions. AG is the centreline, with the radial component of the velocity specified as zero, and zero gradient applied for the vertical component of velocity, zero gradient for both k and ε, and zero gradient for the phase fractions. Initial conditions are specified as zero velocity everywhere in the region, with horizontal interfaces between phases.

Meshing of the model region is performed using custom scripts implementing OpenFOAM's *blockMesh* and *refineMesh* tools. Several levels of mesh refinement are applied in the liquid phases in the vicinity of the impinging jet in the central region of the model, as well as the body of the jet itself. Figure 3b shows an example mesh of the region.

RESULTS AND DISCUSSION

Model validation

In order to study the mesh dependence of the model as well as its accuracy in predicting variables such as the dimensions of the cavity and flow fields formed by the jet impinging on the slag surface, a simplified two-phase test case was constructed using the parameters shown in Table 4. These parameters match those of an air-water model constructed by Zhang et al. [17] for experimental testing, which was also used for computational model testing and verification in the work of Nguyen & Evans [11].

Table 4: Zhang water model parameters

Parameter	*Value*	*Parameter*	*Value*
L_A	0.154 m	L_E	0 m
h_L	0.111 m	h_D	0 m
d_N	0.006 m	d_E	0.006 m
d_F	0.290 m	v_{z0}	56.2 m/s
ρ_G	1.177 kg/m^3	μ_G	1.846 x 10^{-5} Pa.s
ρ_L	992.2 kg/m^3	μ_L	6.578 x 10^{-4} Pa.s
γ_{GL}	0.07 N/m		

Meshes of the model region were constructed at four resolutions ranging from 3434 to 62409 elements. A simulation was performed at each resolution, for a total time of 1 second each. Results from the test case are shown in Figures 4 and 5.

Mesh independence is largely attained with resolutions above 15000 elements. At lower resolutions (eg Figure 4a), it can be seen that the recirculation cells in the gas and liquid phases are located further away

from the axis, and as a result the shape of the liquid surface in the cavity region is also different. Graphically representing the vertical position of the base of the cavity as a function of time confirms this, as the low resolution model predicts very different qualitative behaviour and steady-state values for the cavity. Models with mesh resolutions over 20000 elements were therefore used in all subsequent simulations.

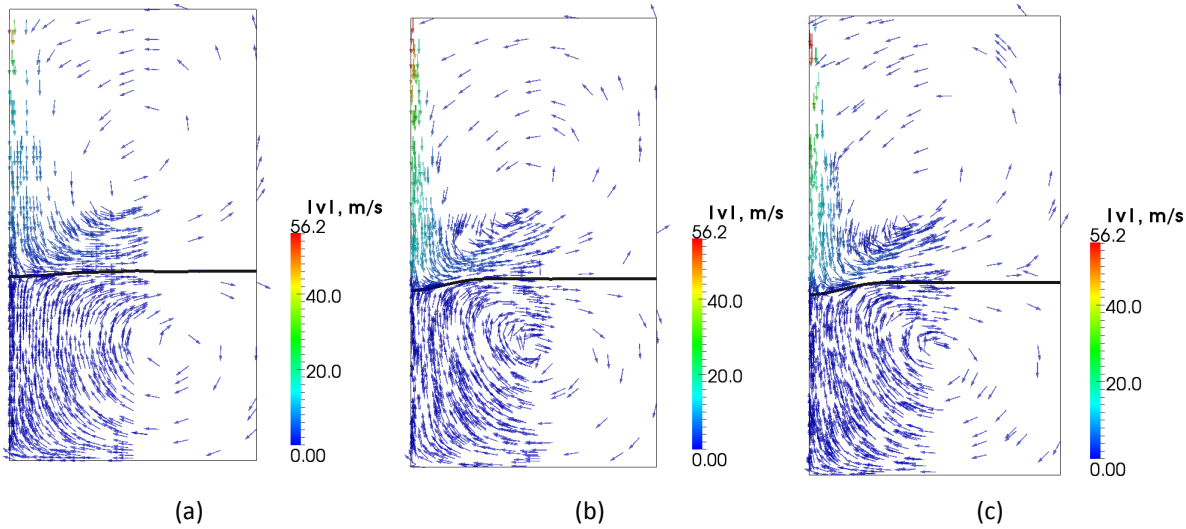

Figure 4: Visualisations of the flow field (unit vectors) and liquid surface (black line) at 1 s for different resolutions, (a) 3434, (b) 15669, (c) 34353 elements

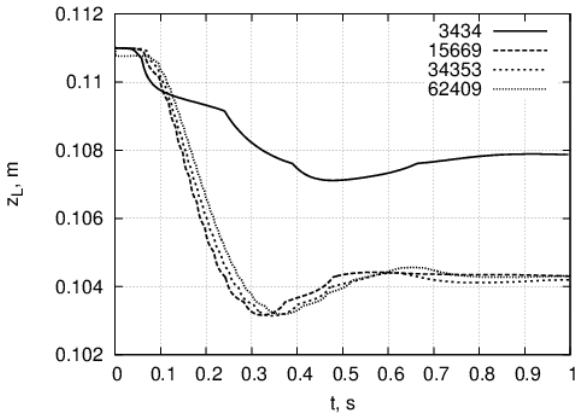

Figure 5: Evolution of z_L with time for different mesh resolutions

An important phenomenon in the arc impingement problem is the effect of the arc length L_A on the dimensions of the cavity formed in the slag, particularly its depth. From observations of DC plasma arcs as well as turbulent jet theory, the jet diameter is expected to increase with increasing length. This causes the thrust force to be spread over a larger area, with the result that the cavity depth should decrease and its diameter increase. This effect was captured succinctly in theory and compared with extensive experimental data by Cheslak et al. [8], who presented the relationship (6) for the cavity depth a (= h_L+h_D-z_L) as a function of N_{Fr}.

$$N_{Fr} = \frac{\pi}{2K^2}\left(\frac{a}{L_A}\right)\left(1+\frac{a}{L_A}\right)^2 \tag{6}$$

In this expression, K is the dimensionless jet decay constant for the centreline velocity in round turbulent jets, and typically takes on values between 5 and 7 (e.g., Or et al. [18]). Fitting of K to the jet velocity field calculated in the test case model produced a value of 5.315.

In order to assess the effect of the jet length on the test case model and compare it with (6), the value of L_A was varied between 0.025 m and 0.25 m while keeping all other parameters shown in Table 4 constant. Once the system had reached steady state with no further changes in the flow patterns or cavity shape, the cavity depth was calculated. The results are given in Table 5.

Table 5: Effect of jet length on cavity depth

Jet length, L_A	*Model cavity depth at 1 s, a*	N_{Fr}	*a/L_A, model*	*a/L_A, eqn (6)*
0.025 m	0.0331 m	0.691	1.32	1.70
0.050 m	0.0250 m	0.0864	0.501	0.607
0.100 m	0.0122 m	0.0108	0.122	0.157
0.154 m	0.00720 m	0.00296	0.0467	0.0484
0.250 m	0.00343 m	0.000691	0.0137	0.0121

The test case models are seen to agree reasonably well with the predictions of equation (6), although there are some discrepancies particularly at short jet lengths where the model underpredicts the cavity depth relative to (6). For the purpose of studying DC arc furnaces, a degree of underprediction is acceptable since this will generally lead to more conservative estimates of bath penetration by the arc, and hence the electrical design of the furnace. Despite the differences, the qualitative behaviour of the model is seen to be very similar to that of (6) – this is shown graphically in Figure 6.

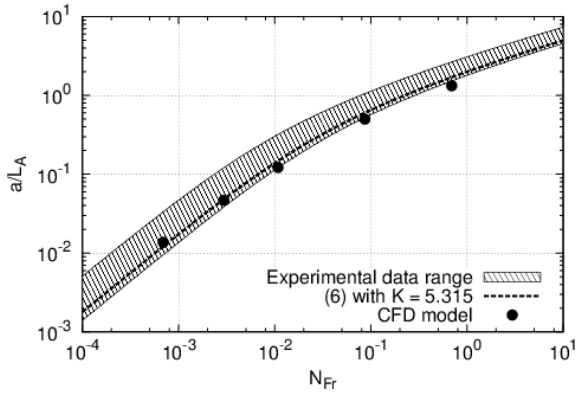

Figure 6: Comparison between Cheslak et al. [8] experimental data ranges, equation (6), and model results

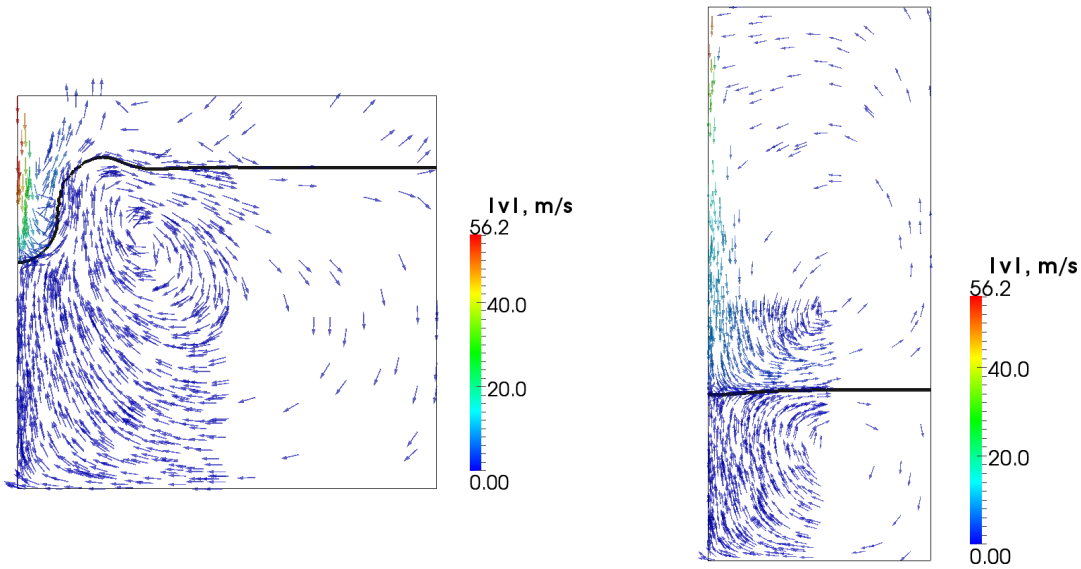

(a) (b)

Figure 7: Visualisations of fluid interface (black line) and flow fields (unit vectors) for different jet lengths, (a) 0.025 m and (b) 0.250 m

Visualisations of the velocity field and the gas-liquid interface are shown for long and short jet lengths in Figure 7. A narrower, deeper cavity with a raised lip around the edge is formed in the case of the short jet.

The recirculation vortex surrounding the cavity in the liquid layer is also located much closer to the cavity than in the case of the long jet.

Pilot-scale furnace model results

DC furnaces are often operated at small scale (up to a few megawatts) in order to pilot processes and designs for industrial plants. The scale-up factor between pilot and full scale can be as much as an order of magnitude or more. It is therefore of some interest to examine the behaviour of the model using typical parameters at both scales to identify any significant differences that may be important for the scale-up design. The base case parameter set used for the pilot-scale DC furnace model is shown in Table 6.

Table 6: Base case parameter set for furnace and model systems (at pilot scale)

Parameter	*DC furnace*	*CFD model*	*Parameter*	*DC furnace*	*CFD model*
L_A	0.2 m	0.06 m	L_E	0.167 m	0.05 m
h_L	0.3 m	0.09 m	h_D	0.1 m	0.03 m
d_N	-	0.005 m	d_E	0.2 m	0.06 m
d_F	2.0 m	0.6 m	v_{z0}	-	35.0 m/s
ρ_G	0.00906 kg/m^3	1 kg/m^3	μ_G	1.45 x 10^{-4} Pa.s	1.16 x 10^{-4} Pa.s
ρ_L	3500 kg/m^3	750 kg/m^3	μ_L	0.2 Pa.s	0.16 Pa.s
ρ_D	7000 kg/m^3	1500 kg/m^3	μ_D	6.1 x 10^{-3} Pa.s	4.87 x 10^{-3} Pa.s
γ_{GL}	0.25 N/m	4.82 x 10^{-3} N/m	γ_{LD}	0.75 N/m	0.0145 N/m
I	5 kA	-			

All model parameters are selected such that the dimensionless quantities in Table 1 match those of the actual furnace. The only exception is the ρ_G/ρ_L density ratio, which if maintained would lead to either very high slag phase densities or very low gas phase densities (and hence high jet velocities). In the interests of solution stability and compute time required, a higher gas-phase density was selected – the ρ_G/ρ_L ratio is however still very close to zero, as it is for the real furnace.

Results from the base case pilot furnace model are shown in Figures 8 and 9.

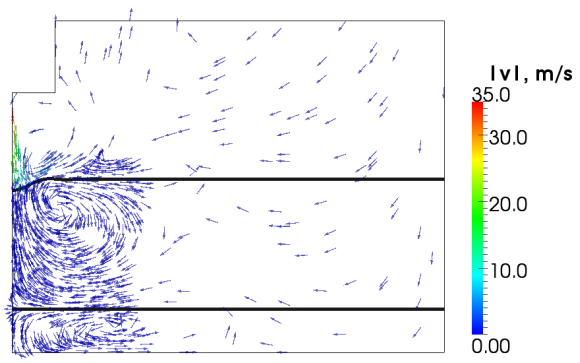

Figure 8: Steady-state phase interfaces (black lines) and velocity field (unit vectors), base case

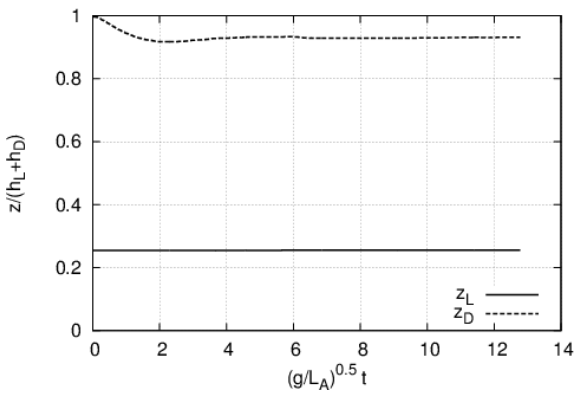

Figure 9: Evolution of slag and metal layer levels with dimensionless time

As can be seen in Figure 8, at 5 kA the thrust of the arc jet creates a noticeable cavity in the surface of the molten slag layer. This is accompanied by a clockwise recirculation cell in the slag phase surrounding the cavity. The resulting flow pattern causes a counter-clockwise recirculation to develop in the metal layer at the bottom of the vessel.

Due to the depth of the slag layer relative to the dimensions of the cavity in this case, the arc does not penetrate through the slag and the metal-slag interface remains relatively undisturbed. This is shown in

Figure 9, which presents the change in the positions of the two phase interfaces over time during the simulation. The final steady-state values for the dimensionless slag and metal levels are 0.931 and 0.255 respectively.

The sensitivity of the pilot-scale model was examined by adjusting several of furnace's key process and design variables one at a time while keeping all other parameters constant as per Table 6. The effect of each parameter on the slag and metal levels in the cavity region was then examined by comparing values before and after arc jet impingement had occurred. The results are shown in Figure 10.

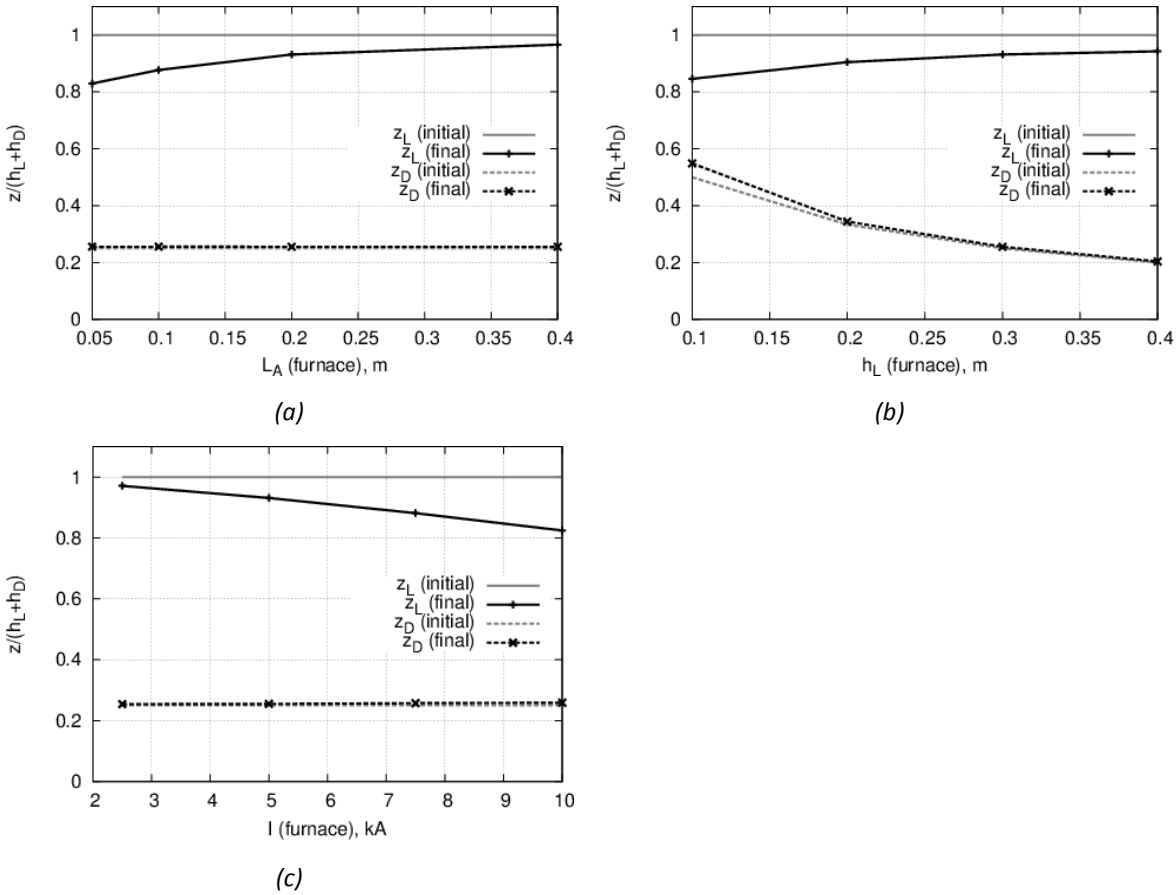

Figure 10: Graphs showing the effect on centreline slag and metal levels at steady state of (a) furnace arc length, (b) furnace slag layer depth, (c) furnace current

Varying the arc length between 5 and 40 cm has very little effect on the final steady-state level of the metal layer in the furnace. Shorter arc lengths are seen to increase the depth of penetration of the arc into the slag, however, a substantial depth of slag always remains between the arc and the metal.

A similar situation obtains from varying the furnace current between 2.5 and 10 kA. Higher currents produce increased penetration depth into the slag layer, consistent with the increase in arc jet thrust that is produced, but very little change in the metal level.

Changing the slag layer depth in the furnace between 10 and 40 cm produces an interesting effect; although the dimensions of the cavity at the slag surface remain more or less constant, at shallow slag depths the counter-clockwise vortex flow that forms in the metal phase becomes strong enough to cause the metal layer near the centre of the furnace (directly beneath the cavity in the slag) to rise upward slightly. This "metal rise" effect has been noted by other workers (e.g., Szekely [19]), but generally in the context of converting or fossil-fuel-fired furnaces using high-velocity gas lances. In the DC arc furnace, any metal rise beneath the arc jet has greater significance as, together with the cavity formed at the slag surface, it causes a reduction in the length of the current path through the slag. This may be expected to affect the overall electrical behaviour of the furnace, although at typical pilot-plant scale the effect is seen to be minimal and is only likely to appear for operations with unusually high currents and shallow slag layers.

Industrial-scale furnace model results

Moving to more typical values for industrial furnaces, a second case was examined using the parameters shown in Table 7.

Table 7: Base case parameter set for furnace and model systems (at industrial scale)

Parameter	*DC furnace*	*CFD model*	*Parameter*	*DC furnace*	*CFD model*
L_A	0.75 m	0.06 m	L_E	0.625 m	0.05 m
h_L	0.75 m	0.06 m	h_D	0.2 m	0.016 m
d_N	-	0.005 m	d_E	0.75 m	0.06 m
d_F	10.0 m	0.8 m	v_{z0}	-	72.3 m/s
ρ_G	0.00906 kg/m^3	1 kg/m^3	μ_G	1.45 x 10^{-4} Pa.s	1.60 x 10^{-5} Pa.s
ρ_L	3500 kg/m^3	750 kg/m^3	μ_L	0.2 Pa.s	0.022 Pa.s
ρ_D	7000 kg/m^3	1500 kg/m^3	μ_D	6.1 x 10^{-3} Pa.s	6.71 x 10^{-4} Pa.s
γ_{GL}	0.25 N/m	3.43 x 10^{-4} N/m	γ_{LD}	0.75 N/m	1.03 x 10^{-3} N/m
I	75 kA	-			

As before, all model parameters are chosen such that the dimensionless parameters in Table 1 match those of the real furnace, with the exception of the gas-slag density ratio. Results from the model are shown in Figures 11 and 12.

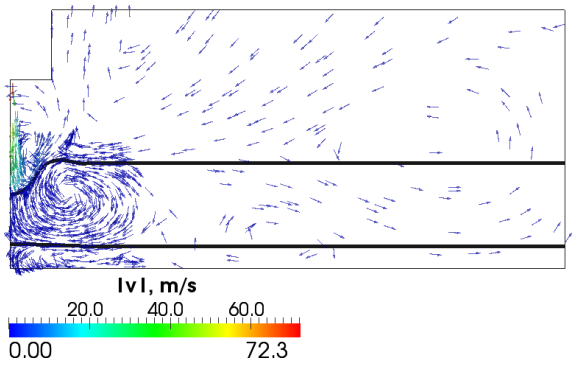

Figure 11: Steady-state phase interfaces (black lines) and velocity field (unit vectors), base case

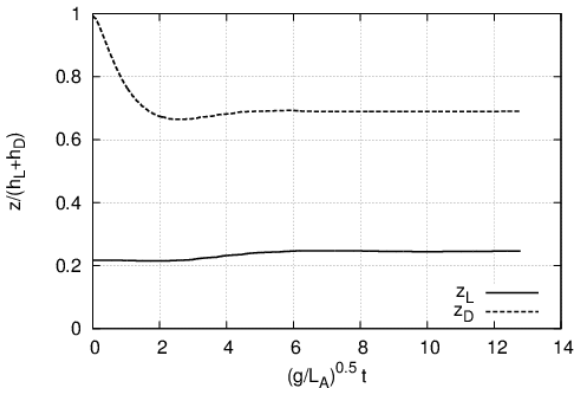

Figure 12: Evolution of slag and metal layer levels with dimensionless time

In the industrial-scale model, the aspect ratio of both slag and metal phase layers is larger than in the pilot operation. The arc jet is therefore able to penetrate further into the liquid bath, and produces a relatively deep, narrow cavity with a significant raised lip at the surface of the slag. The strong vortex circulation formed around the narrow cavity also results in a small but visible metal rise effect, with the metal layer building up at the centre of the furnace beneath the arc impingement zone. The final steady-state values for the dimensionless slag and metal levels are 0.690 and 0.246 respectively.

The sensitivity of the industrial-scale model was examined using the same procedure as for the pilot-scale model, varying several of furnace's key process and design parameters one at a time while keeping the others constant as per Table 7. The effect of each parameter on the slag and metal levels in the cavity region was then examined by comparing values before and after arc jet impingement had occurred. The results are shown in Figure 13.

As expected, altering the arc length between 0.25 m and 1 m has a pronounced effect on the arc jet penetration depth, with cavity depth increasing at shorter arc lengths. Interestingly however, the change in cavity dimensions and associated circulation patterns in the slag and metal layers does not appreciably

affect the steady-state level of the metal layer, which remains more or less constant across the range of arc lengths tested.

Similarly, increasing the furnace current from 50 kA to 125 kA produces an increase in cavity depth to the point that at very high currents the cavity formed by the arc jet is nearly as deep as the slag-metal interface. This is as a result of the increased thrust provided by the arc (cf. equation (2)). The metal rise effect also increases gradually as the current level is raised.

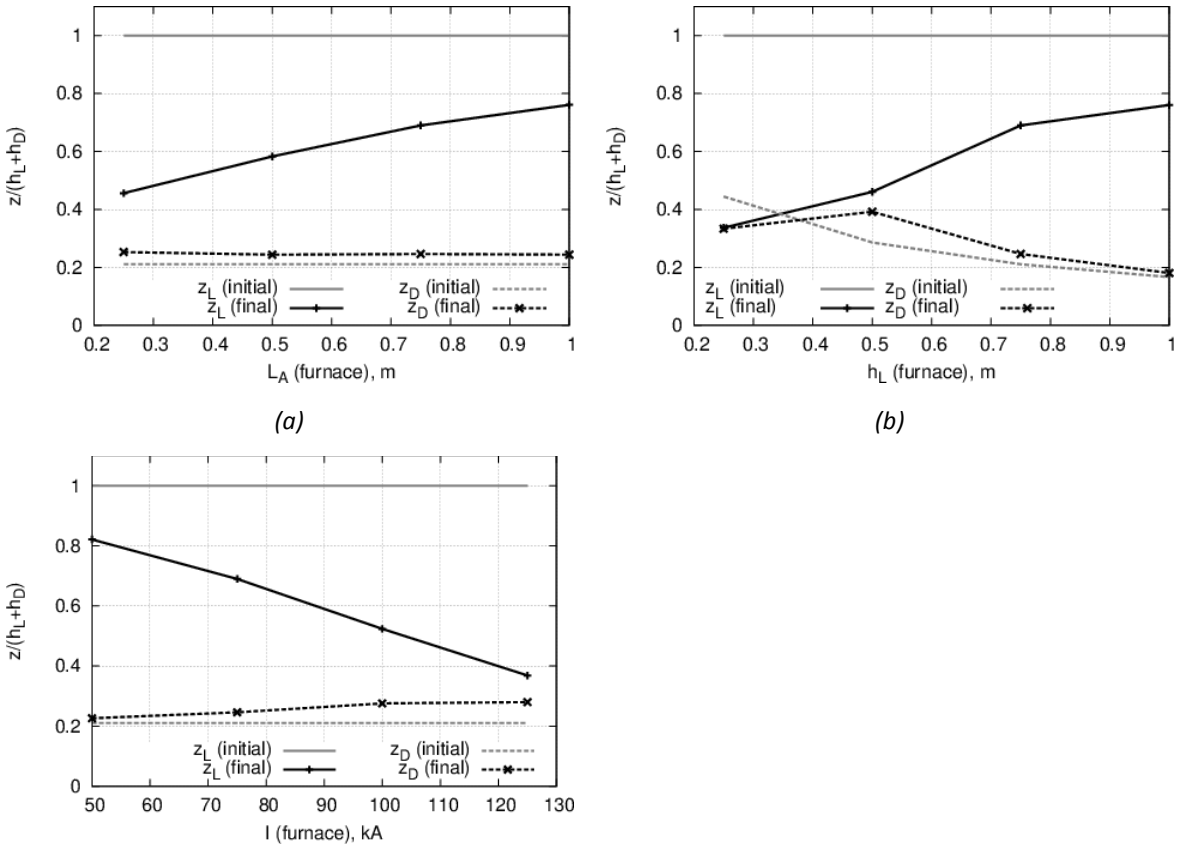

Figure 13: Graphs showing the effect on centreline slag and metal levels at steady state of (a) furnace arc length, (b) furnace slag layer depth, (c) furnace current

Varying the depth of the slag phase produces some highly non-linear behaviour in the model. As slag depth is reduced, the metal rise effect becomes more and more pronounced, until the metal layer is almost in contact with the bottom of the cavity formed in the slag. Further reducing the slag depth then results in complete penetration by the arc jet through the slag and into the metal phase. These two conditions are very significant for the electrical design of DC furnaces, as the arc is able to make direct contact with the highly-conductive metal bath (and hence furnace anode). In both these cases, conduction through the slag layer therefore plays little or no role in contributing to the electrical resistance of the furnace operation. The flow and phase fields at the end of the simulation show the differences between the metal-rise short circuit condition (in Figure 14a) and the slag-penetration short circuit condition (Figure 14b).

The time dependence of the position of the phase interfaces on the centreline of the furnace is shown in Figure 15. Figure 15a shows the development of a metal-rise short circuit condition, with both interfaces converging on a point between their initial values, and Figure 15b shows the development of a slag-penetration short circuit condition, with both moving below the initial slag-metal interface position.

The time scales associated with the evolution of various flow phenomena are quite distinct, particularly in the metal-rise short circuit case (see Figure 15a). Due to the high velocities in the gas phase, the arc jet forms very quickly above the stagnant liquid, $(g/L_A)^{0.5}t \sim 0.02 – 0.05$. The next feature to form is the cavity in the stagnant slag layer, which is fully developed at $(g/L_A)^{0.5}t \sim 2$. Next, the vortex flow around the cavity in

the slag layer begins to grow, and inward flow of the metal toward the axis begins, from $(g/L_A)^{0.5}t$ ~ 2 – 4. By $(g/L_A)^{0.5}t$ ~ 6 – 8, the metal rise has developed fully and flow patterns begin to approach a steady state.

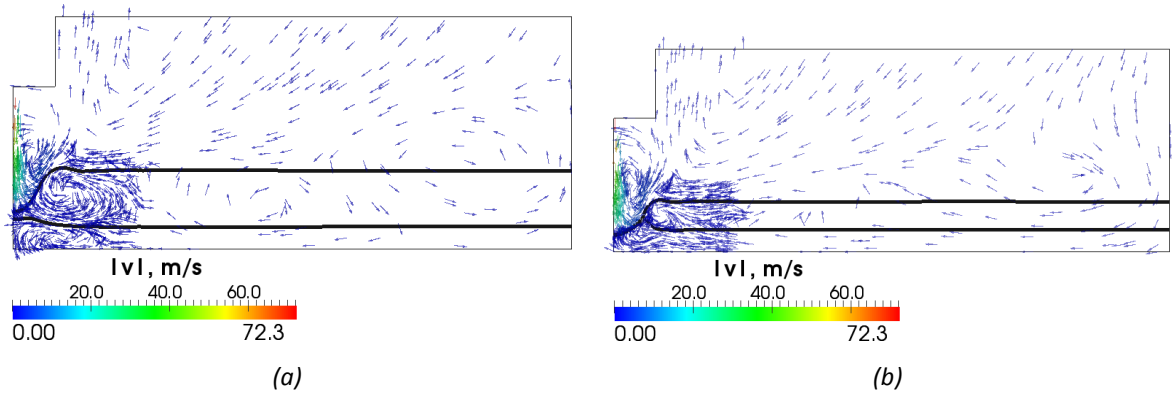

Figure 14: Visualisations of steady-state phase interfaces (black lines) and flow field (unit vectors) for conditions of (a) 50 cm slag depth in furnace, and (b) 25 cm slag depth in furnace

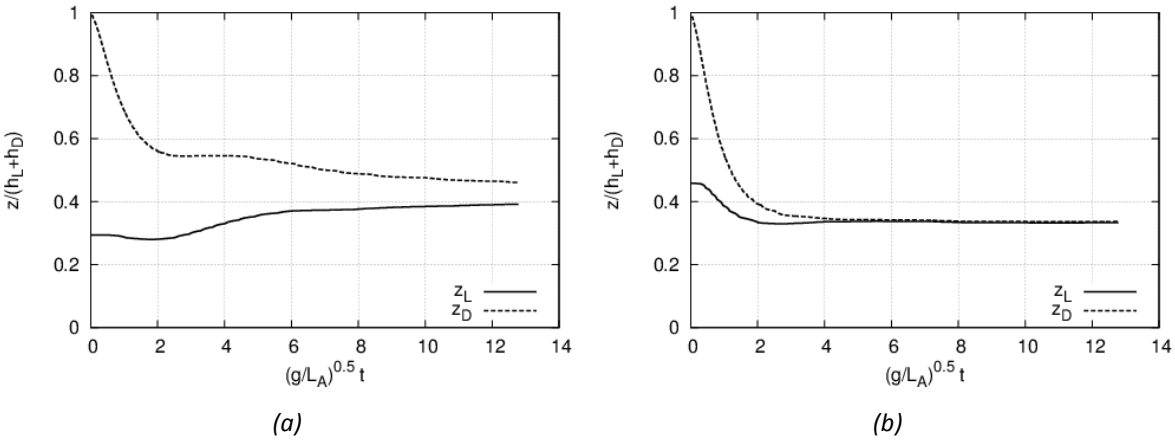

Figure 15: Evolution of slag and metal layer levels with dimensionless time, (a) 50 cm slag depth in furnace, (b) 25 cm slag depth in furnace

These results suggest that the metal-rise short circuit mode in DC arc furnaces may only occur in cases where the arc jet is able to impinge onto a particular location on the slag surface for a significant length of time (2 or more seconds in the industrial-scale example modelled here), whereas the slag-penetration mode can occur considerably faster (0.5 seconds or less). The stability of the arc, and in particular the time scales associated with its erratic motion on the electrode, are therefore expected to have a pronounced effect on the electrical behaviour of the furnace in addition to other design parameters. If the arc stability time scales are within the ranges in which either of the two short circuiting modes can occur, some difficulties with control of the power input to the furnace may be expected – the effective furnace resistance is likely to change significantly every time the arc "jumps" to a new location and has to re-establish the cavity, metal rise, and other flow patterns and phenomena described above.

CONCLUSIONS

Development of a simplified multiphase computational fluid dynamics model to study the phenomenon of arc jet impingement on the molten slag and metal pool in DC arc furnaces has been largely successful. The model was compared to experimental data and theoretical relationships from literature and found to give reasonable predictions of the dimensions of the cavity formed in the liquid surface by the jet. Dimensional similarity considerations were used to specify the parameters for scale models of DC arc furnaces at typical pilot and industrial scale. The scaled models were able to demonstrate several interesting phenomena.

The arcs in typical pilot-scale furnaces generally do not produce enough thrust force to penetrate through the slag or disturb the metal layer below to any significant degree, although cavity formation and fluid recirculation were observed where the arc attaches to the upper part of the slag.

At typical industrial scales, it could be possible for the arc jet to come into direct contact with the metal phase. Two different modes were observed – a fast "slag-penetration" mode in which the arc jet is powerful enough to penetrate deeper than the initial slag-metal interface, and a slower "metal-rise" mode in which the counter-clockwise flow in the metal layer causes the slag-metal interface to rise up and meet the base of the cavity. Contact between the arc jet and the metal would result in short-circuiting of the slag layer, removing a substantial portion of the electrical resistance of the furnace and causing difficulties for the control of power input. This behaviour was seen to be dependent on the furnace design and operating parameters, and would in addition be expected to be affected by the stability of the arc.

Further work in this area would be beneficial to the increased understanding of the arc impingement zone in DC furnaces. Cold model experiments are planned to compare the CFD model with measured data and verify the dimensional scaling behaviour. Enhancement of the present models would also be advisable – currently, the flow model uses a rather basic turbulence formulation, and this could potentially be extended to eddy simulation methods given sufficient computing resources. The inclusion of heat transfer effects, and possibly a full MHD solution, should also be investigated.

ACKNOWLEDGEMENTS

This paper is published by permission of Mintek. Discussion with members of the CSIR Aeronautic Systems group was useful in the completion of this work, as was access to computational facilities at the CSIR's Pretoria campus and the CSIR/Meraka Institute's Centre for High Performance Computing.

REFERENCES

1 Jones, R.T. and Curr, T.R., "Pyrometallurgy at Mintek", Proceedings of Southern African Pyrometallurgy 2006, 5-8 March 2006, Johannesburg (South Africa), pp 127-150, 2006.

2 Alexis, J., Ramirez, M. and Trapaga, G., "Modeling of heat transfer from an electric arc – a simulation of heating Part 1", Proceedings of the 57th Electric Furnace Conference, 14-16 November 1999, Pittsburg (USA), pp 279-290, 1999.

3 Maecker, H., "Plasmastromungen in Lichtbogen infolge eigenmagnetischer Kompression", Zeitschrift fur Physik, vol. 141, pp 198-216, 1955.

4 Bowman, B., "Properties of arcs in DC furnaces", Proceedings of the 52nd Electric Furnace Conference, 13-16 November 1994, Nashville (USA), pp 111-120, 1994.

5 Reynolds, Q.G., Jones, R.T. and Reddy, B.D., "Mathematical and computational modelling of the dynamic behaviour of direct current plasma arcs", Journal of the Southern African Institute of Mining and Metallurgy, vol. 110, pp 733-742, 2010.

6 Jones, R.T., Reynolds, Q.G. and Alport, M.J., "DC arc photography and modelling", Minerals Engineering, vol. 15, no. 11S1, pp 985-991, 2002.

7 Reynolds, Q.G. and Jones, R.T., "Semi-empirical modelling of the electrical behaviour of DC-arc smelting furnaces", Journal of the South African Institute of Mining and Metallurgy, vol. 104, pp 345-351, 2004.

8 Cheslak, F.R., Nicholls, J.A. and Sichel, M., "Cavities formed on liquid surfaces by impinging gaseous jets", Journal of Fluid Mechanics, vol. 36, pt 1, pp 55-63, 1969.

9 Ushio, M., Szekely, J. and Chang, C.W., "Mathematical modelling of flow field and heat transfer in high-current arc discharge", Ironmaking and Steelmaking, no. 6, pp 279-286, 1981.

10 Forrester, S.E. and Evans, G.M., "Computational Modelling Study of a Plane Gas Jet Impinging onto a Liquid Pool", Proceedings of the 1st International Conference on CFD in the Mineral & Metal Processing and Power Generation Industries, 3-4 July 1997, Melbourne (Australia), pp 313-320, 1997.

11 Nguyen, A.V. and Evans, G.M., "Computational fluid dynamics modelling of gas jets impinging onto liquid pools", Applied Mathematical Modelling, vol. 30, pp 1472-1484, 2006.

12 Bowman, B., “Convective heat transfer and power balance in high current free-burning arcs”, Elektrowarme International, no. 30, pp B 87 – B 93, 1972.
13 Bowman, B., “MHD effects in arc furnaces”, Proceedings of the IUTAM Symposium on Metallurgical Applications of Magnetohydrodynamics, Cambridge (UK), pp 272-282, 1982.
14 OpenFOAM 2.1.1, http://www.openfoam.org
15 Launder, B. E., and Sharma, B. I., "Application of the Energy Dissipation Model of Turbulence to the Calculation of Flow Near a Spinning Disc", Letters in Heat and Mass Transfer, vol. 1, no. 2, pp 131-138, 1974.
16 Hirt, C.W. and Nichols, B.D., "Volume of fluid (VOF) method for the dynamics of free boundaries", Journal of Computational Physics, vol. 39, no. 1, pp 201–225, 1981.
17 Zhang, J., Du, S. and Wei, S., “Flow field in bath agitated by symmetrically placed impinging jet and submerged gas stream”, Ironmaking and Steelmaking, no. 6, pp 249-255, 1985.
18 Or, C.M., Lam, K.M. and Liu, P., “Potential core lengths of round jets in stagnant and moving environments”, Journal of Hydro-environment Research, no. 5, pp 81-91, 2011.
19 Szekely, J., “Fluid flow phenomena in metal processing”, Academic Press Inc., Waltham (USA), 1980.